



Article

A Novel Intelligent Condition Monitoring Framework of Essential Service Water Pumps

Yingqian Liu ¹, Qian Huang ², Huairui Li ¹, Yunpeng Li ¹, Sihan Li ¹, Rongsheng Zhu ¹ and Qiang Fu ^{1,*}

¹ Research Center of Fluid Machinery Engineering & Technology, Jiangsu University, Zhenjiang 212013, China; 2112111007@stmail.ujs.edu.cn (Y.L.); leehuirui@126.com (H.L.); airocyli@126.com (Y.L.); 15702446994@163.com (S.L.); zrs@ujs.edu.cn (R.Z.)

² China Nuclear Power Engineering Co., Ltd., Beijing 100840, China; huangqian@cnpe.cc

* Correspondence: ujsfq@outlook.com; Tel.: +86-15240287004

Abstract: Essential service water pumps are necessary safety devices responsible for discharging waste heat from containments through seawater; their condition monitoring is critical for the safe and stable operation of seaside nuclear power plants. However, it is difficult to directly apply existing intelligent methods to these pumps. Therefore, an intelligent condition monitoring framework is designed, including the parallel implementation of unsupervised anomaly detection and fault diagnosis. A model preselection algorithm based on the highest validation accuracy is proposed for anomaly detection and fault diagnosis model selection among existing models. A novel information integration algorithm is proposed to fuse the output of anomaly detection and fault diagnosis. According to the experimental results of modules, a kernel principal component analysis using mean fusion processing multi-channel data (AKPCA (fusion)) is selected, and a support vector machine using mean fusion processing multi-channel data (SVM (fusion)) is selected. The overall test accuracy and false negative rate of AKPCA (fusion) are 0.83 and 0.144, respectively, and the overall test accuracy and f_1 -score of SVM (fusion) are 0.966 and 1, respectively. The test results of AKPCA (fusion), SVM (fusion), and the proposed information integration algorithm show that the information integration algorithm successfully avoids a lack of abnormal status information and misdiagnosis. The proposed framework is a meaningful attempt to achieve the intelligent condition monitoring of complex equipment.

Keywords: essential service water pumps; model preselection algorithm; unsupervised anomaly detection; fault diagnosis; intelligent condition monitoring



Citation: Liu, Y.; Huang, Q.; Li, H.; Li, Y.; Li, S.; Zhu, R.; Fu, Q. A Novel Intelligent Condition Monitoring Framework of Essential Service Water Pumps. *Appl. Syst. Innov.* **2024**, *7*, 61. <https://doi.org/10.3390/asi7040061>

Received: 18 June 2024
Revised: 16 July 2024
Accepted: 17 July 2024
Published: 19 July 2024



Copyright: © 2024 by the authors. Licensee MDPI, Basel, Switzerland. This article is an open access article distributed under the terms and conditions of the Creative Commons Attribution (CC BY) license (<https://creativecommons.org/licenses/by/4.0/>).

1. Introduction

Essential service water pumps (ESWPs) play a crucial role in seaside nuclear power plants (SNPPs), which are responsible for transmitting waste heat through seawater. If an ESWP malfunctions without preparation, it is likely to cause nuclear safety issues due to the inability to discharge waste heat promptly. Its condition monitoring is essential for the predictive maintenance of SNPPs [1] and the production of clean and efficient nuclear energy [2]. On the one hand, its condition monitoring ensures the regular transfer of waste heat and maintains the safe and stable operation of the entire SNPP. On the other hand, it is essential to prepare spare parts like sealing rings and bearings in time according to condition monitoring to prevent shutdowns due to the failure of spare parts to arrive in time, affecting production.

Present intelligent condition monitoring methods using equipment's historical data align more with predictive maintenance requirements [3], mainly including anomaly detection (AD) and fault diagnosis (FD). There are many unsupervised AD (UAD) methods [4], such as support vector data description (SVDD) [5], k-nearest neighbor clustering [6], dynamic time warping [7], and anomaly detection based on kernel principal component

analysis (AKPCA) [8]. Although some AD models based on deep learning have been studied [9,10], most lack further investigation, except for their network design. Relying on these networks will not only fail to solve current problems but may also lead to new problems, such as the explainability and computational complexity of deep learning models. FD aims to obtain status information about equipment based on learning data. Previous research has been conducted to identify pumps' faults, such as misalignment [9], lack of balance [10], bearing defects [11], leakage [12], etc. Focused on feature extraction, a complex feature extraction method composed of continuous wavelet transform, a multilayer feedforward perceptron neural network, and a genetic algorithm has been used by many researchers to prepare valuable features for support vector machines (SVMs) classifying both mechanical and hydraulic faults of centrifugal pumps [10]. Focused on deep learning networks, some researchers converted non-image signals into image signals [13,14] for neural networks and extracted features using deep networks instead of traditional feature extraction methods [15].

The above research mainly focused on ordinary pumps. Intelligent condition monitoring research on SNPPs has received increasing attention in recent years. For instance, a deep convolutional conditional generative adversarial network was designed to process imbalanced sample problems of motors and bearings [16]. A deep residual neural network was combined with a transferred vibration image to utilize multi-sensor vibration signals to diagnose the motor and bearing [17]. A novel Artificial Disturbance Method (ADM)-based domain discrepancy generalization promotion framework was proposed, significantly enhancing the generalization ability of convolutional neural networks (CNNs) in nuclear power plant fault diagnosis [18]. A hybrid methodology that integrated knowledge-based methods, quantitative mathematical models, and data-driven methodologies was used to meet the complex need for different parts of SNPPs [19]. A Q network calibrated ensemble method was used to realize the fault diagnosis of a nuclear Circulating Water Pump Gearbox, which focused on the problem of imbalanced samples and shaft distribution [20]. Although these studies obtained some satisfying results, it is still hard to apply deep learning models [21].

Most existing UAD algorithms can find anomalies lacking details, and most existing intelligent FD algorithms can only intelligently diagnose faults that have been learned by the model and cause the misdiagnosis of faults that have not been learned. Predictive maintenance needs to find out whether the equipment is in abnormal operation and specific information about the abnormal operation to guide maintenance. Therefore, AD and FD algorithms are equally important in supporting predictive maintenance. Although there are some intelligent methods including both AD and FD [22,23], or methods focused on unknown faults [24], they are currently not considering how to select the most suitable model among existing models quickly, and the question of how to fuse the different outputs of UAD and FD lacks research. This paper aims to provide an intelligent condition monitoring framework for ESWPs. To achieve this aim, a unique condition monitoring framework based on UAD and FD parallel implementation is proposed, and a model pump of an ESWP with five-channel vibration is built for essential data collection and model testing. Multi-channel data put together (together) or fused by mean fusion (fusion) are two attempted signal processing methods for UAD and FD. A model preselection algorithm based on the highest validation accuracy has been proposed to select the best UAD model from common UAD models and the best FD model from common classifiers. Expert intervention is suggested to support the updating of models for persistence. The contributions of this paper include the following:

1. A model preselection algorithm is proposed to select the best model among existing models.
2. An information integration algorithm is proposed to integrate the output of UAD and FD to avoid misdetection and misdiagnosis.
3. The condition monitoring framework obtained by the parallel connection of UAD and FD provides a new method for obtaining the status of complex critical equipment.

The remainder of this paper is organized as follows: The main theory related to basic UAD and FD models is introduced in Section 2. The test bench, dataset, and the proposed intelligent condition monitoring method are described in Section 3. All module and overall experiment results and related discussions are presented and analyzed in Section 4. Finally, the main conclusions are given in Section 5.

2. Basic Theory

2.1. Unsupervised Anomaly Detection Algorithms

One-class SVM (OCSVM) tries to find a hyperplane with a maximum margin by almost all positive training samples to separate negative samples as far as possible [25]. Due to the nonlinear separability of samples in ordinary space, samples are usually converted into linearly separable samples through projection functions φ . The hyperplane can be expressed as

$$f(x_i) = w^T \varphi(x_i) - b \tag{1}$$

where w^T is a normal vector representing weight, b is offset, and $f(x_i)$ is the classifier's output under input x_i . The optimization problem can be described as

$$\begin{aligned} \min_{w,b,\xi} & \left(\|w\|_2^2 + \frac{1}{vn} \sum_{i=1}^N \xi_i - b \right) \\ \text{s.t.} & (w^T \varphi(x_i)) \geq b - \xi_i, \xi_i \geq 0, i = \{1, 2, \dots, N\} \end{aligned} \tag{2}$$

where $v \in (0, 1]$, and ξ_i is the slack variable that balances boundary positions and classification errors, making the model more flexible and robust when dealing with incomplete linearly separable data. To obtain the solution to the optimization problem, the dual problem is

$$\begin{aligned} \min_{\alpha} & (-0.5\alpha^T \alpha) \\ & \sum_{i=1}^N \alpha_i = 1 \\ \text{s.t.} & 0 \leq \alpha_i \leq \frac{1}{vn} \end{aligned} \tag{3}$$

where α represents the Lagrange multiplier. After calculating the offset b and the weight w , the state of the sample is determined by the relationship between the sample and the hyperplane.

AKPCA has illustrated that reconstruction error (Squared Prediction Error, *SPE*) with the RBF kernel can detect a sample exceeding the healthy operating range and a sample that does not follow the training data model [8]. For training data $X = \{x_i | i = \{1, 2, \dots, N\}\}$, the *SPE* is defined by the second-order norm of the difference between the centered kernel feature $\tilde{\Phi}(\tilde{x}_j)$ and the reconstruction kernel feature $\hat{\Phi}(\tilde{x}_j)$.

$$SPE_j = \|\tilde{\Phi}(\tilde{x}_j) - \hat{\Phi}(\tilde{x}_j)\|_2 \tag{4}$$

The second-order norm can be calculated by kernel matrix K by

$$\|\tilde{\Phi}(\tilde{x}_j)\|_2 = 1 - 2\bar{K}_j + \bar{K} \tag{5}$$

where K is composed of $K_{i,j} = \Phi(x_i)\Phi(x_j)$, \bar{K}_j represents the average value of the j -th row in K , and \bar{K} represents the average value of all elements in K . According to the relationship of the projection matrix and kernel principal components, *SPE* for KPCA can be written explicitly, as follows:

$$SPE_j = 1 - 2\bar{K}_j + \bar{K} - y_j^T y_j \tag{6}$$

where y_j is the kernel principal component obtained from the eigenvectors and kernel matrix. The upper control limit is the 95-th percentile of $SPE_j, j = \{1, 2, \dots, N\}$ [26]. To judge whether a sample is normal or abnormal, the *SPE* in the kernel space of the sample

can be calculated and compared with the upper control SPE_{limit} . When $SPE_j > SPE_{limit}$, the j – th sample is abnormal, and vice versa.

Isolation forest (ISF) is an anomaly detection algorithm that isolates observations by randomly partitioning the data using binary trees, efficiently identifying anomalies with low computational cost [27]. The root node contains all samples randomly selected from the training dataset X for each tree. There are internal and external nodes, and every internal node is split into two sub-nodes (left and right) until sample isolation is completed or the maximum tree depth is reached: $d_{max} = \log_2(\phi)$ After building the ISF, the following is calculated:

$$\begin{aligned}
 H(n - 1) &= \ln(n - 1) + 0.57721564 \\
 c(n) &= 2(H(n - 1) - (n - 1)/n) \\
 s(x_j, n) &= 2^{-E(h(x_j))/c(n)}
 \end{aligned}
 \tag{7}$$

where $H(n)$ is the harmonic number, $c(n)$ is the average path length, $E(h(x_j))$ is the average of $h(x_j)$, and $s(x_j, n)$ is the anomaly score of x_j in X . The criteria for judging normality or abnormality according to s are shown in Table 1.

Table 1. The criteria of anomaly detection based on ISF.

Criteria	Status
s close to 1 (>0.5)	Abnormal
s approximately equal to 0.5	Normal
s close to 0	Normal

2.2. Fault Diagnosis Algorithms

Convolutional neural networks (CNNs) and SVMs are classical classifying algorithms for supervised FD methods. CNNs were initially proposed for image-related works, and they have been improved and applied in non-image-related works [13,28]. The structure of a CNN includes the input layer, convolutional layers, pooling layers, fully connected layers, the dropout layer, and the output layer. The input and output layers are only responsible for transmitting data without processing. Convolutional layers are the core part of convolutional neural networks which extract features from input data. A pooling layer is added between the two convolutional layers to reduce the parameters of the neural network and prevent overfitting. Generally, each convolutional layer is followed by a ReLU function to accelerate learning and simplify models. The full connection layer converts the output from the convolution and pooling layers into classification or regression results. The dropout layer randomly discards some neurons during the training process to prevent overfitting of the model and improve the generalization ability of the model. The output layer outputs the final result according to the full connection layer.

Originally, SVMs were binary classification mathematical models based on structural risk minimization [29], and they already have been developed to solve multi-class classification problems. One-versus-rest (OVR) and one-versus-one (OVO) are the two main approaches for the multi-class classification of SVMs. The basis of both methods is to transform a multi-class problem into multiple binary classification problems. For training samples $\{(x_i, y_i) | x_i \in \mathbb{R}^m, i = \{1, 2, \dots, N\}, y_i \in \{-1, 1\}\}$, SVM linear classifiers complete the classification task by placing a hyperplane between samples x_i of two linearly separable categories. An SVM nonlinear classifier introduces kernel function to project the nonlinearly separable samples x_i into a separable projected feature $\varphi(x_i)$, similar to the processing of SVDD models. Since the principles of the linear and nonlinear classification of SVMs are similar, nonlinear classification is introduced here. The decision function can be expressed as

$$f(x_i) = w^T \varphi(x_i) - b
 \tag{8}$$

where w^T and b are adjustable parameters of the decision function, and $f(x_i)$ is the output of the classifier with input x_i . The optimization problem is converted by constructing the hinge loss function

$$\min_{w,b,\xi} \left(\|w\|_2^2 + \frac{1}{C} \sum_{i=1}^N \xi_i \right) \tag{9}$$

$$s.t. y_i(w^T \varphi(x_i) - b) \geq 1 - \xi_i, \xi_i \geq 0, i = \{1, 2, \dots, N\}$$

where C is the penalty factor and ξ_i is a relaxation variable. Introducing Lagrange multiplier technology, the dual problem of Equation (9) is

$$\max_{\alpha} \left(\sum_{i=1}^N \alpha_i - \frac{1}{2} \sum_{i=1}^N \sum_{j=1}^N \alpha_i \alpha_j y_i y_j K(x_i, x_j) \right) \tag{10}$$

$$s.t. \sum_{i=1}^N \alpha_i y_i = 0$$

$$\frac{1}{2n\lambda} \geq \alpha_i \geq 0, i = 1, \dots, N$$

where α_i are the Lagrange multipliers; then,

$$b = w^T \varphi(x_i) - y_i = \left[\sum_{j=1}^N \alpha_j y_j K(x_j, x_i) - y_i \right] \tag{11}$$

Finally, the decision function is

$$f(z) = \text{sgn} \left(w^T (\varphi(z) - b) \right) = \text{sgn} \left(\left[\sum_{i=1}^N \alpha_i y_i K(x_i, z) \right] - b \right) \tag{12}$$

where $\text{sgn}()$ means symbolic function. For a sample z , the predicted label is $f(z)$. And the $f(z)$ of multi-classes are processed by OVR [30]. We will choose the better one between the CNN and the SVM through cross-validation and the model preselection algorithm.

3. Methodology

3.1. Test Bench and Data Description

To obtain a condition monitoring framework suitable for ESWPs, we built a model pump test bench for an ESWP for data collection and validation; the main parameters of the model pump are shown in Table 2. Due to the power of the test bench pump being lower than 200 kW, vibration measurement points are set according to the Chinese standard GB/T 6075.7-2015 [31] and actual needs. The test bench and vibration measuring points are shown in Figure 1. Five channels of the water pump are measured, and the main parameters of the model pump are shown in Table 2.

Table 2. Main design point parameters of the model pump.

Parameter	Value
N	2900 revolutions per minute (rpm)
H	20 m
Q	100 m ³ /h
P	6.80 kW

Where N represents the rated speed of the motor, H represents the pump head, Q represents the rated flow rate, and P represents the rated power of the driven motor.

The vibration data collected from the test bench include data representing normal status, coupling misalignment, mass imbalance, casing ring wear, blade wear (one blade wear), and bench instability. Before each fault is prefabricated, 40 s of normal status data are collected before each fault, and 10 s data of each fault are collected, respectively. Each sampling includes three channels of vibration acceleration signals from the bearing (in the x, y, and z directions) and two channels of vibration acceleration signals from the motor (in the x and y directions), all with a sampling rate of 10.24 kHz. The designed speed of the test pump is 2900 rpm, and the sample length is suggested to satisfy the Nyquist Sampling

Theorem, set as 1250 points (0.122 s). This sample length is enough for the designed speed or a much lower operating speed in practice operating. The sample usage of UAD and FD is shown in Table 3. Moreover, 10 s of strong blade wear (2-blade wear) data are collected, and 10% of samples are randomly selected to test the proposed framework.

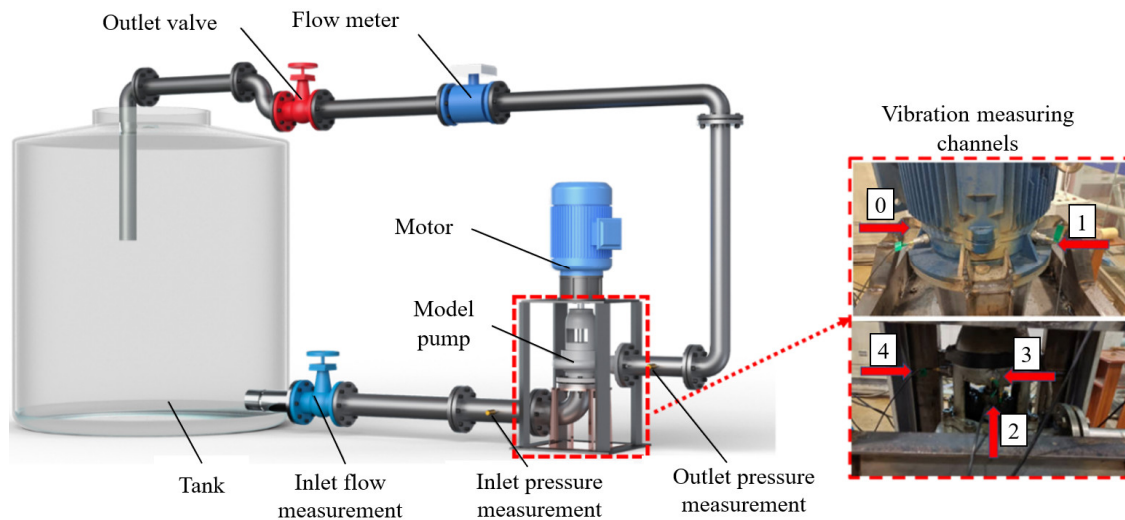


Figure 1. Schematic diagram of model pump device and vibration measuring points, ‘0’ and ‘1’ represent two measuring points on the motor, ‘2’, ‘3’, and ‘4’ represent three measuring points on the bearing near the pump.

Table 3. The basic sample requirement for modeling.

Data Type	Sample Number of Each Channel	Anomaly Detection	Fault Identification
Normal (Nor)	320	70% training, 20% validation, 10% test	Randomly select 80 samples, 70% training, 20% validation, 10% test
Coupling misalignment (CM)	80		70% training, 20% validation, 10% test
Mass imbalance (MI)	80		70% training, 20% validation, 10% test
Casing ring wear (CRW)	80	80% validation, 20% test	70% training, 20% validation, 10% test
Blade wear (BW)	80		70% training, 20% validation, 10% test
Bench instability (BI)	80		70% training, 20% validation, 10% test

3.2. Multi-Channel Data Processing

Critical equipment generally has multi-channel data, and analyzing and modeling each channel’s data requires a large workforce and a lot of material resources. However, the question of how to directly apply all channels’ data to the model is also a problem that needs to be studied. Two ways are introduced here. One is to put the samples of all channels together (together). Another is to apply all channels’ data by mean fusion (fusion). The samples from 5 channels are processed using these two methods, as shown in Figures 2 and 3. Ch means channel, left signals represent raw signals, right signals/signal are/is the processed signal.

The distinct difference between the two methods is the number of samples. The number of samples directly put together is five times the number of mean fusion methods, and the sample count for the mean fusion method is shown in Table 3. After that, the method TFF_VMD mentioned in reference [23] is used to extract features as the input of subsequent models. Some of these features have been used to detect mechanical bearing faults [32], hydraulic blockage faults [33], and cavitation [34,35]. Briefly, the statistical features of time series and the Fast Fourier Transfer amplitude spectrum and three power spectrum features are extracted by FFT_VMD from both the raw sample and its five

Intrinsic Mode Functions of Variable Mode Decomposition and strung together as the simplified sample.

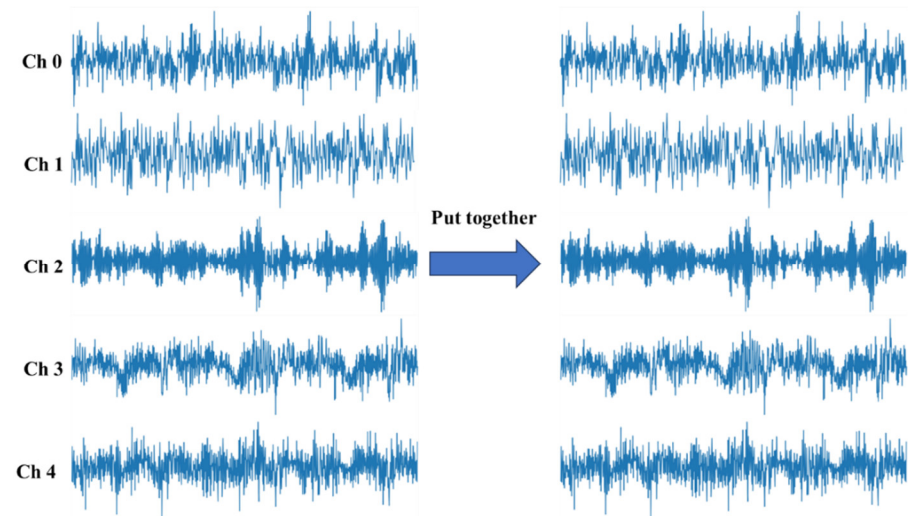


Figure 2. Putting samples of all channels together.

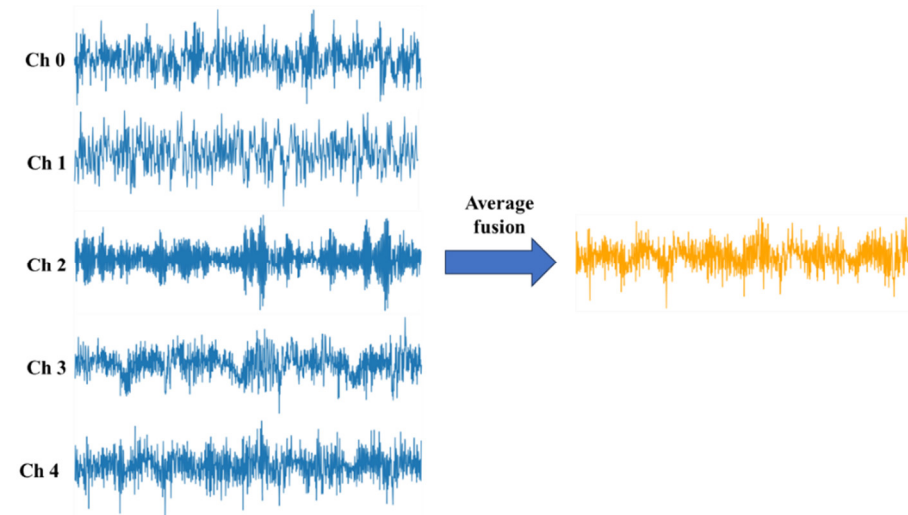


Figure 3. Fusing all channels' samples with mean fusion.

3.3. Model Preselection Algorithm

Plenty of intelligent models exist, so we should choose the most suitable one for application through the model preselection algorithm from at least two typical models. The validation accuracy of the model is considered in the model preselection algorithm. The model selection process is mathematically defined as follows:

$$\begin{aligned}
 & Sel(M_1, M_2, \dots, M_p) = M_i \\
 & s.t. \max(M_{1-valid-acc}, M_{2-valid-acc}, \dots, M_{p-valid-acc}) = M_{i-valid-acc}
 \end{aligned} \tag{13}$$

where M_i represents the i -th model of the provided p models. $M_{i-valid-acc}$ represents the validation accuracy of M_i . If the multi-fold cross-validation is applied, $M_{i-valid-acc}$ represents the mean of multi-fold cross-validation accuracy. The accuracy can be calculated by

$$Accuracy = \frac{TP + TN}{TP + TN + FP + FN} \tag{14}$$

TP means the number of samples correctly detected or diagnosed as positive, FN means the number of samples incorrectly detected or diagnosed as negative, TN means the number of samples correctly identified or diagnosed as negative, and FP means the number of samples incorrectly detected or diagnosed as positive.

The model with the highest validation accuracy is selected, and the accuracy should be greater than 0.8 according to the standard GB/T 43555-2023 [36] to ensure the selected UAD and FD models are valid. The process can be described in Figure 4. Model M_i is the most suitable model for the same dataset and performs best among the provided p models.

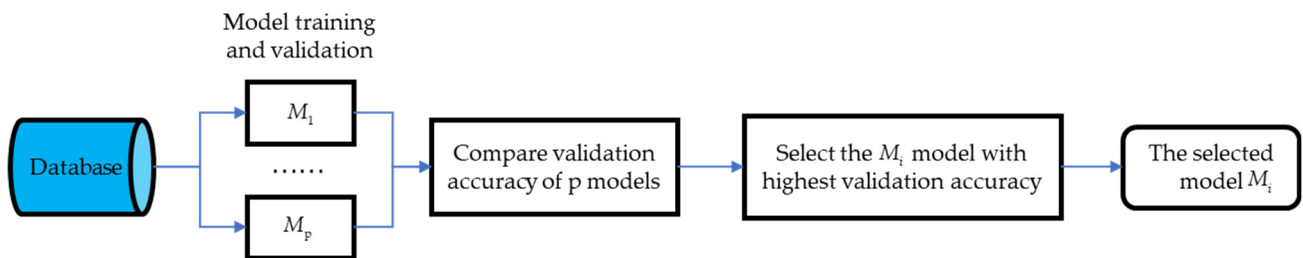


Figure 4. The model preselection process.

3.4. Information Integration Algorithm

For the UAD model, the anomaly detection rate (ADR) indicates the proportion of samples detected as abnormal by UAD in the batch of test samples. If the ADR is greater than 10% [23], the output of UAD is regarded as abnormal. Otherwise, the output is regarded as normal status. The output of FD is the most probable status (MPS) and its probability (P_MPS). Due to the different output formats and contents of UAD and FD, they cannot be directly fused. However, as mentioned above, practical applications must combine these results to provide more comprehensive decision support. Therefore, the information integration algorithm is proposed to fuse the results of UAD and FD, as shown in Algorithm 1. The key idea is to use the consistent information of AD and FD, and experts would deeply analyze the inconsistent results. Notably, 80% of P_MPS used is based on the GB/T 43555-2023 [36] standard.

Algorithm 1. Information integration algorithm.

Input: a batch of detection samples X_{test}

Output: status and decision

1. get ADR of UAD based on X_{test}
 2. get MPS and P_MPS of FD based on X_{test}
 3. **if** $ADR < 10\%$ & MPS is normal status **then**
 4. go on condition monitoring
 5. **if** $ADR \geq 10\%$ & MPS is a specific fault & $P_MPS \geq 80\%$ **then**
 6. control based on MPS
 7. **otherwise**
 8. expert analysis, go on monitoring, control the pump, or supplement data according to analysis results
 9. **End**
-

3.5. The Condition Monitoring Method

Based on the methods mentioned in Sections 3.2–3.4, the whole framework for condition monitoring can be described as shown in Figure 5. The black line mainly represents the offline model building process, the green line represents the online condition monitoring process, the red line represents the control operation, and the yellow bottom part represents the common part of both UAD and FD. Considering the problem of an incomplete fault dataset, UAD is conducted in parallel with FD, which requires only normal status data to build the model. FD is realized with at least two balanced data types (including

normal status data). The bottom content related to the expert is flexible according to the analysis results.

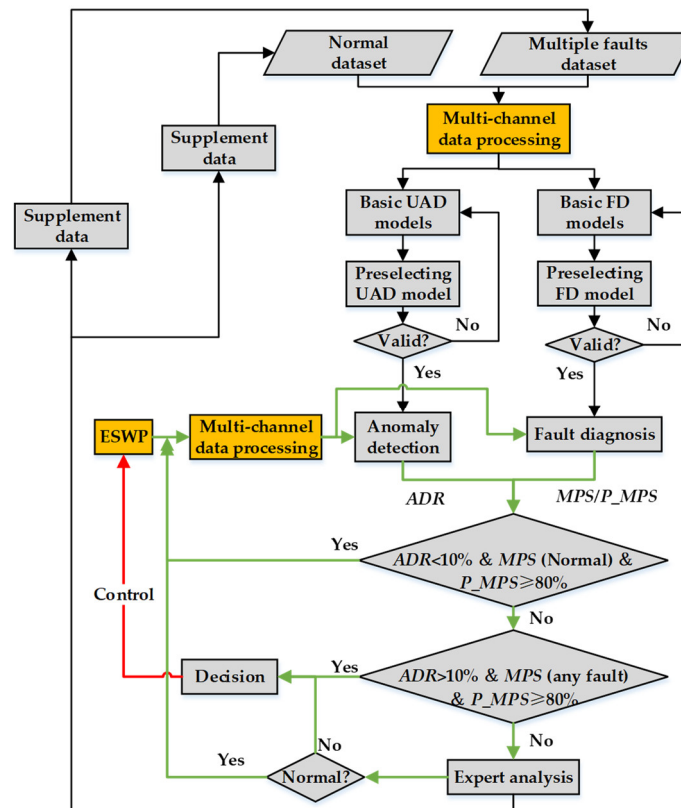


Figure 5. The ESWP condition monitoring framework based on UAD and FD.

4. Experiment Results and Discussion

4.1. UAD Model Preselection Results

The dataset in Table 3 is used to train and validate UAD models mentioned in Section 2.1 with the proposed model preselection method in Section 3.3 to select the most suitable UAD model. The validation false negative rate (FNR) of different UAD models is calculated by Equation (15), except for validation accuracy, to help prove the reliability of the proposed preselection method.

$$FNR = \frac{FN}{TP + FN} \tag{15}$$

Table 4 shows the ten-fold cross-validation accuracy obtained by different UAD methods on multi-channel data, and Table 5 presents the corresponding FNR. The bold data indicate the highest cross-validation accuracy and the lowest FNR. According to the results in Table 4, AKPCA (fusion) achieves the highest mean ten-fold cross-validation accuracy at 0.83, making it the most suitable UAD model as selected by the model preselection algorithm. Table 5 shows that AKPCA (fusion) also achieves the lowest FNR at 0.144. Although ISF (fusion) attains a mean accuracy greater than 0.8 and a mean FNR less than 0.4, its performance is still inferior to that of AKPCA (fusion). FNR is another evaluation indicator in addition to accuracy; an FNR of 0.4 is the qualified limit for determining whether an anomaly detection model is acceptable.

Table 4. The accuracy results of validation samples.

Fold	1	2	3	4	5	6	7	8	9	10	Mean
OCSVM (together)	0.356	0.342	0.356	0.342	0.375	0.368	0.38	0.382	0.384	0.383	0.367
OCSVM (fusion)	0.56	0.564	0.56	0.564	0.502	0.547	0.559	0.555	0.517	0.534	0.546
AKPCA (together)	0.717	0.705	0.717	0.705	0.717	0.711	0.734	0.737	0.733	0.732	0.721
AKPCA (fusion)	0.871	0.872	0.871	0.872	0.862	0.852	0.866	0.85	0.69	0.7	0.83
ISF (together)	0.419	0.453	0.431	0.428	0.483	0.467	0.466	0.461	0.446	0.481	0.793
ISF (fusion)	0.817	0.821	0.841	0.828	0.793	0.826	0.831	0.845	0.798	0.767	0.817

Table 5. The FNR results of validation samples.

Fold	1	2	3	4	5	6	7	8	9	10	Mean
OCSVM (together)	0.926	0.924	0.926	0.924	0.929	0.928	0.928	0.929	0.929	0.929	0.927
OCSVM (fusion)	0.643	0.641	0.643	0.641	0.615	0.638	0.659	0.667	0.654	0.651	0.645
AKPCA (together)	0.38	0.391	0.38	0.391	0.384	0.387	0.385	0.383	0.379	0.371	0.383
AKPCA (fusion)	0.148	0.146	0.148	0.146	0.12	0.146	0.146	0.146	0.146	0.146	0.144
ISF (together)	0.815	0.772	0.804	0.802	0.748	0.768	0.802	0.811	0.829	0.777	0.453
ISF (fusion)	0.237	0.221	0.203	0.227	0.229	0.224	0.227	0.229	0.234	0.245	0.227

4.2. FD Model Preselection Results

To select a suitable FD model and signal preprocessing method, the SVM and one-dimensional CNN (1DCNN) are trained and validated based on the experimental data, and the structure and main parameters of the trained 1DCNN are recorded in Table 6. The main parameters of the SVM referred to in [23] are used here, as shown in Table 7.

Table 6. The structure and parameters of the 1DCNN.

Layer Type	Specific Setup	Parameters Number	Output Shape
Input layer	Sample length = 162	0	(None, 162, 1)
Conv1D_1 (ReLU)	Filters = 16, kernel size = 9, stride = 1	160	(None, 154, 16)
Pooling_1	Max pooling size = 2, stride = 1	0	(None, 77, 16)
Conv1D_2 (ReLU)	Filters = 32, kernel size = 5, stride = 1	2592	(None, 73, 32)
Pooling_2	Max pooling size = 2, stride = 1	0	(None, 36, 32)
Conv1D_3 (ReLU)	Filters = 64, kernel size = 3, stride = 1	6208	(None, 34, 64)
Flatten	-	0	(None, 2176)
FC (ReLU)	-	139,328	(None, 64)
Dropout	0.5	0	(None, 64)
FC (ReLU)	-	2080	(None, 32)
Dropout	0.5	0	(None, 32)
FC (SoftMax)	-	198	(None, 6)

FC: full connection.

Table 7. The parameters of SVM.

Parameters	SVM
Gamma	0.16
C	0.9
Kernel	'linear'

The validation accuracy results of the 1DCNN and SVM with different multi-signal processing methods are recorded in Table 8. From this table, the mean of the ten-fold cross-validation accuracy results of all SVM and 1DCNN models are larger than 0.8. The mean accuracy of 1DCNN (fusion) and SVM (fusion) is very close to 1, while the mean accuracy of 1DCNN (together) and SVM (together) is less than 0.9, which means the mean fusion method should be selected. According to the model preselection algorithm, SVM

(fusion) with the highest mean value of cross-validation accuracy (0.996) is regarded as the best FD model.

Table 8. The ten-fold cross-validation accuracy results comparison of 1DCNN and SVM.

Fold	1	2	3	4	5	6	7	8	9	10	Mean
1DCNN (together)	0.927	0.967	0.764	0.931	0.915	0.876	0.963	0.941	0.912	0.711	0.89
1DCNN (fusion)	0.997	1	0.996	0.997	0.992	0.996	0.997	0.999	0.996	0.963	0.993
SVM (together)	0.842	0.842	0.842	0.842	0.842	0.842	0.842	0.842	0.842	0.842	0.842
SVM (fusion)	0.996	0.996	0.996	0.996	0.996	0.996	0.996	0.996	0.996	0.996	0.996

The processing of multi-channel signals herein differs from that in reference [37]. Directly inputting multi-channel data into neural networks could achieve good results, subject to the size of the dataset. f_1 -score is the evaluation parameter composed of *Precision* and *Recall*; the calculation is realized by Equations (16)–(18). The f_1 -score results of the 1DCNN and SVM with different multi-channel data processing are recorded in Table 9.

$$Precision = \frac{TP}{TP + FP} \tag{16}$$

$$Recall = \frac{TP}{TP + FN} \tag{17}$$

$$f_1 - score = \frac{2 \times Precision \times Recall}{Precision + Recall} \tag{18}$$

Table 9. The f_1 -score results of the ten-fold cross-validation of the 1DCNN and SVM.

Fold	1	2	3	4	5	6	7	8	9	10	Mean
1DCNN (together)	0.924	0.962	0.781	0.918	0.917	0.859	0.962	0.922	0.91	0.748	0.89
1DCNN (fusion)	1	1	1	1	1	1	1	1	1	0.974	0.997
SVM (together)	0.838	0.838	0.838	0.838	0.838	0.838	0.838	0.838	0.838	0.838	0.838
SVM (fusion)	1	1	1	1	1	1	1	1	1	1	1

4.3. The Test Results of the Whole Condition Monitoring Method

Based on the results of the above models with two methods utilizing multi-channel vibration data on the validation dataset, the mean fusion is selected as the multi-channel data processing method, and AKPCA is selected as the UAD model, while the SVM is selected as the FD model. Therefore, the framework consists of AKPCA and the SVM within mean fusion processing five channels of vibration signals, as shown in Figure 6.

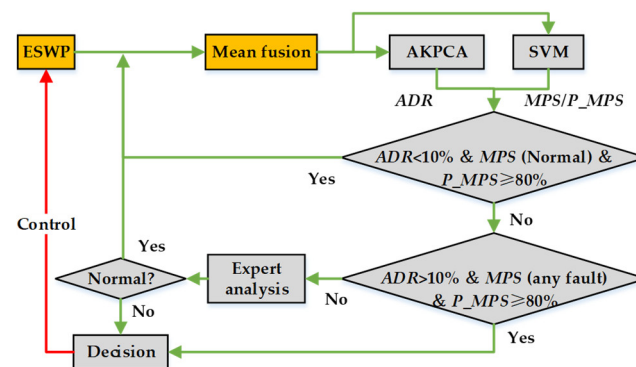


Figure 6. The online condition monitoring model with specific algorithms.

After obtaining the detailed models of the framework, all samples' test results accuracy and *FNR* of AKPCA (fusion) are 0.83 and 0.144. All samples' test results in terms of the accuracy and f_1 -score of SVM (fusion) are 0.996 and 1. The confusion matrix of SVM (fusion) is shown in Figure 7. The confusion matrix shows that most faults are diagnosed correctly, but 16.7% of coupling misalignment (CM) and 16.7% of casing ring wear (CRW) samples are misdiagnosed. The diagnostic accuracy of SVM (fusion) for each fault is greater than 0.8, which meets the GB/T 43555-2023 [36] standard requirement for qualified models. That is, SVM (fusion) models are qualified.

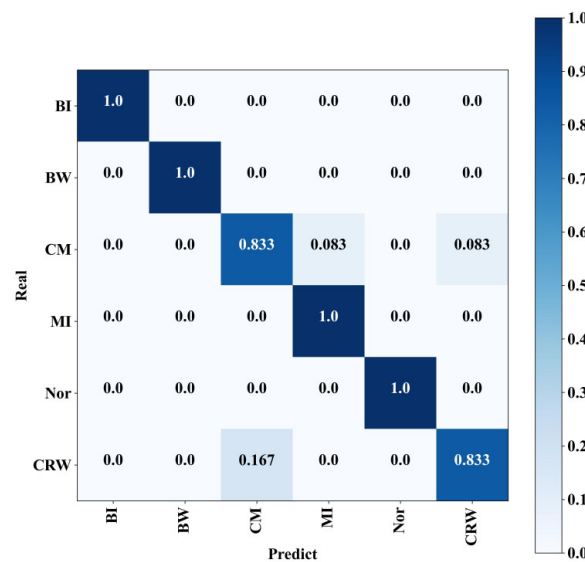


Figure 7. The confusion matrix of SVM (fusion) on the test dataset.

Each status's test samples are independently evaluated using the entire framework, with results detailed in Table 10. According to AKPCA's findings, the model successfully identified coupling misalignment, mass eccentricity, casing ring wear, blade wear, bench instability, and strong blade wear (two-blade wear, not learned by the SVM), all with *ADR* exceeding 10% [23]. However, normal status samples, with an *ADR* of 11%, were incorrectly detected as abnormal status samples.

Table 10. The results of AKPCA (fusion), SVM (fusion), and the information integration algorithm on different status samples.

Test Data's Status	ADR (AKPCA (Fusion))	MPS, P_MPS (SVM (Fusion))	Information Integration Results
Normal	11%	Normal, 100%	Expert analysis
Coupling misalignment	43.8%	Coupling misalignment, 87.5%	Coupling misalignment
Mass eccentricity	11%	Mass eccentricity, 94%	Mass eccentricity
Casing ring wear	16%	Casing ring wear, 88%	Casing ring wear
Blade wear	19%	Blade wear, 100%	Blade wear
Bench instability	100%	Bench instability, 100%	Bench instability
Strong blade wear	97.9%	Bench instability 58.3%	Expert analysis

In the SVM's results, the unlearned strong blade wear fault was identified as bench instability with 58.3% probability, while other faults were diagnosed correctly with probabilities exceeding 80%. No abnormal status information would be obtained in scenarios where only a UAD module is available. Conversely, if only an FD model were used, the unlearned fault might be misclassified as one of the learned faults, resulting in a misdiagnosis.

By employing the information integration algorithm, consistent results from both the UAD and FD models accurately identify all classical faults with 100% accuracy. Inconsistent results, such as normal status and unlearned strong blade wear, are flagged for expert

analysis. In summary, the integration resolves missing abnormal status information from the anomaly detection model and solve misdiagnosis problems arising from the fault diagnosis model.

4.4. Discussion

In Section 4, the highest test accuracy (0.83) and smallest *FNR* (0.144) obtained by AKPCA (fusion) shows that AKPCA is the best UAD method among OCSVM (together), OCSVM (fusion), AKPCA (together), AKPCA (fusion), ISF (together), and ISF (fusion). Similarly, the highest accuracy (0.996) and highest f_1 -score (1) of SVM (fusion) shows that SVM (fusion) is the best model among 1DCNN (together), 1DCNN (fusion), SVM (together), and SVM (fusion). The test results prove that selecting a model based on the highest validation accuracy is reliable. In addition, mean fusion is a good choice for multi-channel same-type signal processing and is helpful for UAD and FD.

The results in Table 10 illustrate that only AKPCA results in a lack of specific fault information when an anomaly is detected, while using only SVM may lead to misdiagnosis. These issues are resolved when AKPCA and SVM operate in parallel through the information integration algorithm. Therefore, within a framework where UAD and FD function in parallel, the information integration algorithm is essential for the comprehensive and precise condition monitoring of complex equipment, including but not limited to ESWPs. To our knowledge, there is no research on ESWP condition monitoring. The condition monitoring of other types of pumps generally only includes anomaly detection [38] or only includes fault diagnosis [10]. Research on the simultaneous use of UAD and FD has appeared. Reference [39] uses pressurized water reactor simulator data to perform AKPCA and SVM, equivalent to UAD and FD working in series. The design of UAD and FD in series is similar to [23]. This method does not consider the impact of the UAD algorithm's false negatives on the monitored object. Our novel features and innovation lie in the parallel design of UAD and FD algorithms. Compared with the probability-weighted voting decision [40] for the same output form of models, the information integration algorithm focuses on fusing the outputs of models with similar functions but different forms of results. Similar to the ensemble learning mentioned in reference [41], the information integration algorithm is fault-tolerant.

5. Conclusions

This paper proposes a condition monitoring framework, and the models used were trained and tested on the experimental dataset. The test results in Section 4 prove that the aim of the proposed condition monitoring framework for ESWP is achieved, classical faults are found with 100% correct fault information, and the unlearned fault is found and sent to an expert for detailed information. Three conclusions can be drawn: (1) mean fusion is a good choice for multi-channel same-type signal processing. (2) The model preselection algorithm helps filter the most suitable UAD and FD models across existing models. (3) The information integration algorithm helps avoid lacks in specific fault information and misdiagnoses. The proposed condition monitoring framework's novelty is the parallel working of UAD and FD, the model preselection algorithm, and the information integration algorithm.

The shortcoming of this method is that improving the framework requires expert assistance. Further work includes the fusion of different-format results from different models in depth and implementing an expert system. In addition, requesting actual pump data from SNPPs is another essential task to validate and improve the condition monitoring framework. We will continue to focus on the parallel implementation of anomaly detection and fault identification methods in the future. This method can concentrate on different models' advantages and avoid limitations, especially for monitoring critical and complex equipment conditions.

Author Contributions: Conceptualization, Y.L. (Yingqian Liu) and Q.F.; data curation, Q.H.; formal analysis, R.Z.; funding acquisition, Q.F.; investigation, Q.H.; methodology, Y.L. (Yingqian Liu) and Q.F.; project administration, Q.F.; resources, Q.F.; software, Y.L. (Yingqian Liu), Y.L. (Yunpeng Li), and S.L.; supervision, Q.F.; validation, Y.L. (Yingqian Liu) and H.L.; visualization, Y.L. (Yingqian Liu); writing—original draft, Y.L. (Yingqian Liu); writing—review and editing, Q.F. All authors have read and agreed to the published version of the manuscript.

Funding: This research was funded by the National Natural Science Foundation of China, grant number U20A20292.

Data Availability Statement: Restrictions apply to the datasets. The datasets presented in this article are not readily available because the data are part of an ongoing study. Requests to access the datasets should be directed to Professor Qiang Fu, ujsfq@outlook.com.

Conflicts of Interest: The authors declare no conflicts of interest.

Nomenclature

ESWPs	Essential service water pumps
SNPPs	Seaside nuclear power plants
AD	Anomaly detection
FD	Fault diagnosis
UAD	Unsupervised anomaly detection
SVDD	Support vector data description
AKPCA	Anomaly detection based on kernel principal component analysis
SVM	Support vector machine
OCSVM	One-class support vector machine
SPE	Squared Prediction Error
ISF	Isolation forest
CNN	Convolutional neural network
OVR	One-versus-rest
ADR	Anomaly detection rate
MPS	Most probable status
P_{MPS}	Probability of the most probable status
1DCNN	One-dimensional convolutional neural network

References

- Feng, Y.; Wu, X.; Lou, S.; Song, X.; Hong, Z.; Hu, B.; Wang, L.; Si, H.; Tan, J. Design optimization for pressurized water reactor using improved quantum fish swarm algorithm and intuitionistic linguistic decision-making. *Adv. Eng. Inform.* **2024**, *59*, 102315. [[CrossRef](#)]
- Liu, X.; Cheng, W.; Xing, J.; Chen, X.; Li, L.; Guan, Y.; Ding, B.; Nie, Z.; Zhang, R.; Zhi, Y. Predictive maintenance system for high-end equipment in nuclear power plant under limited degradation knowledge. *Adv. Eng. Inform.* **2024**, *61*, 102506. [[CrossRef](#)]
- Zhu, L.; Li, Z.; Chen, J. Evaluating and predicting energy efficiency using slow feature partial least squares method for large-scale chemical plants. *Energy* **2021**, *230*, 120582. [[CrossRef](#)]
- Li, J.; Izakian, H.; Pedrycz, W.; Jamal, I. Clustering-based anomaly detection in multivariate time series data. *Appl. Soft Comput.* **2021**, *100*, 106919. [[CrossRef](#)]
- Yang, J.; Yang, F.; Zhang, L.; Li, R.; Jiang, S.; Wang, G.; Zhang, L.; Zeng, Z. Bridge health anomaly detection using deep support vector data description. *Neurocomputing* **2021**, *444*, 170–178. [[CrossRef](#)]
- Yang, J.; Tan, X.; Rahardja, S. Outlier detection: How to Select k for k-nearest-neighbors-based outlier detectors. *Pattern Recognit. Lett.* **2023**, *174*, 112–117. [[CrossRef](#)]
- Kloska, M.; Grmanova, G.; Rozinajova, V. Expert enhanced dynamic time warping based anomaly detection. *Expert Syst. Appl.* **2023**, *225*, 120030. [[CrossRef](#)]
- Tan, R.; Ottewill, J.R.; Thornhill, N.F. Monitoring statistics and tuning of kernel principal component analysis with radial basis function kernels. *IEEE Access* **2020**, *8*, 198328–198342. [[CrossRef](#)]
- Meng, L.; Zhao, M.; Cui, Z.; Zhang, X.; Zhong, S. Empirical mode reconstruction: Preserving intrinsic components in data augmentation for intelligent fault diagnosis of civil aviation hydraulic pumps. *Comput. Ind.* **2022**, *134*, 103557. [[CrossRef](#)]
- Al-Tubi, M.; Bevan, G.P.; Wallace, P.A.; Harrison, D.K.; Ramachandran, K.P. Fault diagnosis of a centrifugal pump using MLP-GABP and SVM with CWT. *J. Eng. Sci. Technol.* **2019**, *22*, 854–861. [[CrossRef](#)]
- Jamadar, I.M.; Bellary, S.A.I.; Kanai, R.A.; Alrobaian, A.A. Model-Based Condition Monitoring for the Detection of Failure of a Ball Bearing in a Centrifugal Pump. *J. Fail. Anal. Prev.* **2019**, *19*, 1556–1568. [[CrossRef](#)]

12. Chen, X.; Liu, H.; Nikitas, N. Internal pump leakage detection of the hydraulic systems with highly incomplete flow data. *Adv. Eng. Inform.* **2023**, *56*, 101974. [[CrossRef](#)]
13. Tang, S.; Zhu, Y.; Yuan, S. A novel adaptive convolutional neural network for fault diagnosis of hydraulic piston pump with acoustic images. *Adv. Eng. Inform.* **2022**, *52*, 101554. [[CrossRef](#)]
14. Kumar, A.; Gandhi, C.; Zhou, Y.; Kumar, R.; Xiang, J. Improved deep convolution neural network (CNN) for the identification of defects in the centrifugal pump using acoustic images. *Appl. Acoust.* **2020**, *167*, 107399. [[CrossRef](#)]
15. Gao, Y.; Kim, C.H.; Kim, J.-M. A novel hybrid deep learning method for fault diagnosis of rotating machinery based on extended WDCNN and long short-term memory. *Sensors* **2021**, *21*, 6614. [[CrossRef](#)]
16. Wang, Z.; Xia, H.; Zhang, J.; Yang, B.; Yin, W. Imbalanced sample fault diagnosis method for rotating machinery in nuclear power plants based on deep convolutional conditional generative adversarial network. *Nucl. Eng. Technol.* **2023**, *55*, 2096–2106. [[CrossRef](#)]
17. Yin, W.; Xia, H.; Wang, Z.; Yang, B.; Zhang, J.; Jiang, Y.; Miyombo, M.E. A fault diagnosis of nuclear power plant rotating machinery based on multi-sensor and deep residual neural network. *Ann. Nucl. Energy* **2023**, *185*, 109700. [[CrossRef](#)]
18. Lin, M.; Li, J.; Li, Y.; Wang, X.; Jin, C.; Chen, J. Generalization analysis and improvement of CNN-based nuclear power plant fault diagnosis model under varying power levels. *Energy* **2023**, *282*, 128905. [[CrossRef](#)]
19. Liu, Y.-K.; Xie, C.-L.; Peng, M.-J.; Ling, S.-H. Improvement of fault diagnosis efficiency in nuclear power plants using hybrid intelligence approach. *Prog. Nucl. Energy* **2014**, *76*, 122–136. [[CrossRef](#)]
20. Cheng, W.; Wang, S.; Liu, Y.; Chen, X.; Nie, Z.; Xing, J.; Zhang, R.; Huang, Q. A Novel Planetary Gearbox Fault Diagnosis Method for Nuclear Circulating Water Pump With Class Imbalance and Data Distribution Shift. *IEEE Trans. Instrum. Meas.* **2023**, *72*, 1–13. [[CrossRef](#)]
21. Du, Z.; Liang, X.; Chen, S.; Zhu, X.; Chen, K.; Jin, X. Knowledge-infused deep learning diagnosis model with self-assessment for smart management in HVAC systems. *Energy* **2023**, *263*, 125969. [[CrossRef](#)]
22. Elshenawy, L.M.; Halawa, M.A.; Mahmoud, T.A.; Awad, H.A.; Abdo, M.I. Unsupervised machine learning techniques for fault detection and diagnosis in nuclear power plants. *Prog. Nucl. Energy* **2021**, *142*, 103990. [[CrossRef](#)]
23. Liu, Y.; Zhang, R.; He, Z.; Huang, Q.; Zhu, R.; Li, H.; Fu, Q. The study of hydraulic machinery condition monitoring based on anomaly detection and fault diagnosis. *Measurement* **2024**, *230*, 114518. [[CrossRef](#)]
24. Li, J.; Meng, L.; Wang, B.; Tian, R.; Tan, S.; Li, Y.; Chen, J. Open set recognition fault diagnosis framework based on convolutional prototype learning network for nuclear power plants. *Energy* **2023**, *290*, 130101. [[CrossRef](#)]
25. Schölkopf, B.; Platt, J.C.; Shawe-Taylor, J.; Smola, A.J.; Williamson, R.C. Estimating the support of a high-dimensional distribution. *Neural Comput.* **2001**, *13*, 1443–1471. [[CrossRef](#)] [[PubMed](#)]
26. Nomikos, P.; MacGregor, J.F. Multivariate SPC charts for monitoring batch processes. *Technometrics* **1995**, *37*, 41–59. [[CrossRef](#)]
27. Liu, F.T.; Ting, K.M.; Zhou, Z.-H. Isolation-based anomaly detection. *ACM Trans. Knowl. Discov. Data (TKDD)* **2012**, *6*, 1–39. [[CrossRef](#)]
28. Gu, J.; Wang, Z.; Kuen, J.; Ma, L.; Shahroudy, A.; Shuai, B.; Liu, T.; Wang, X.; Wang, G.; Cai, J.; et al. Recent advances in convolutional neural networks. *Pattern Recogn.* **2018**, *77*, 354–377. [[CrossRef](#)]
29. Vapnik, V.N. An overview of statistical learning theory. *IEEE Trans. Neural Netw.* **1999**, *10*, 988–999. [[CrossRef](#)]
30. Xu, J. An extended one-versus-rest support vector machine for multi-label classification. *Neurocomputing* **2011**, *74*, 3114–3124. [[CrossRef](#)]
31. GB/T 6075.7-2015; Mechanical Vibration—Evaluation of Machine Vibration by Measurements on Non-Rotating Parts—Part 7: Rotodynamic Pumps for Industrial Applications, Including Measurements on Rotating Shafts. Standards Press of China: Beijing, China, 2015.
32. Wang, X.-B.; Zhang, X.; Li, Z.; Wu, J. Ensemble extreme learning machines for compound-fault diagnosis of rotating machinery. *Knowl. Based Syst.* **2020**, *188*, 105012. [[CrossRef](#)]
33. Kumar, D.; Dewangan, A.; Tiwari, R.; Bordoloi, D. Identification of inlet pipe blockage level in centrifugal pump over a range of speeds by deep learning algorithm using multi-source data. *Measurement* **2021**, *186*, 110146. [[CrossRef](#)]
34. Tiwari, R.; Bordoloi, D.; Dewangan, A. Blockage and cavitation detection in centrifugal pumps from dynamic pressure signal using deep learning algorithm. *Measurement* **2021**, *173*, 108676. [[CrossRef](#)]
35. Al-Obaidi, A.R. Detection of cavitation phenomenon within a centrifugal pump based on vibration analysis technique in both time and frequency domains. *Exp. Tech.* **2020**, *44*, 329–347. [[CrossRef](#)]
36. GB/T 43555-2023; Intelligent Service—Predictive Maintenance—Algorithm Evaluation Method. Standards Press of China: Beijing, China, 2023.
37. Tang, S.; Zhu, Y.; Yuan, S. An improved convolutional neural network with an adaptable learning rate towards multi-signal fault diagnosis of hydraulic piston pump. *Adv. Eng. Inform.* **2021**, *50*, 101406. [[CrossRef](#)]
38. Liang, X.; Duan, F.; Bennett, I.; Mba, D. A Sparse Autoencoder-Based Unsupervised Scheme for Pump Fault Detection and Isolation. *Appl. Sci.* **2020**, *10*, 6789. [[CrossRef](#)]
39. Hang, W.; Peng, M.; Yu, Y.; Saeed, H.; Hao, C.; Liu, Y. Fault identification and diagnosis based on KPCA and similarity clustering for nuclear power plants. *Ann. Nucl. Energy* **2021**, *150*, 107786. [[CrossRef](#)]

40. Rojarath, A.; Songpan, W. Probability-weighted voting ensemble learning for classification model. *J. Adv. Inf. Technol.* **2020**, *11*, 217–227. [[CrossRef](#)]
41. Zhong, X.; Ban, H. Crack fault diagnosis of rotating machine in nuclear power plant based on ensemble learning. *Ann. Nucl. Energy* **2022**, *168*, 108909. [[CrossRef](#)]

Disclaimer/Publisher’s Note: The statements, opinions and data contained in all publications are solely those of the individual author(s) and contributor(s) and not of MDPI and/or the editor(s). MDPI and/or the editor(s) disclaim responsibility for any injury to people or property resulting from any ideas, methods, instructions or products referred to in the content.